Avalanche process of the fiber-bundle model with stick-slip dynamics and a variable Young modulus

Da-Peng Hao,* Gang Tang,† Hui Xia, Zhi-Peng Xun, and Kui Han
Department of Physics, China University of Mining and Technology, Xuzhou 221116, People's Republic of China
(Received 11 January 2013; published 26 April 2013)

In order to more accurately describe the fracture process of extensive biological fibers, a fiber-bundle model with stick-slip dynamics and a variable Young modulus is constructed. In this model, the Young modulus of a fiber is assumed to increase or decrease by multiplying with a changing ratio after local sliding events. So, the maximum number of stick-slip events of a single fiber and the changing ratio of the Young modulus are the two key parameters of the model. By means of analytical theory and numerical simulation, the constitutive law, the critical stress, the average size of the largest avalanche, and the avalanche size distribution are shown against the two parameters of the model. From a macroscopic viewpoint, the constitutive curves show different morphologies varying from a local plastic state to a unimodal parabola, while from a microscopic viewpoint, the avalanche size distributions can be well fitted into a power law relationship, which is in accord with the classical fiber-bundle model.

DOI: 10.1103/PhysRevE.87.042126 PACS number(s): 64.60.Ht, 46.50.+a, 62.20.M−, 81.40.Np

I. INTRODUCTION

Fracture and material stability have attracted many technological and industrial interests for a long time. Due to the inherent nonuniformity and disorder in actual materials, the theoretical approach of statistical physics is widely used to investigate the properties of the ruptures and their microscopic mechanisms. The presence of disorder introduces strong fluctuations based on statistical properties [1]. Most of the statistical investigations on the rupture of disordered materials rely on the fiber-bundle model (FBM), which, in most cases, can capture correctly the collective static and dynamic properties of fracture failure in loaded materials. The algorithm of the FBM is so simple that it is possible to obtain exact results analytically or trustable statistical properties numerically [2,3].

The FBM consists of a set of parallel fibers whose breaking strengths are assumed to be randomly dispersed. The bundle is loaded parallel to the fiber direction. The fibers fail if the load on them exceeds their threshold value. Under stress-controlled loading conditions, after each fiber failure, the load carried by the broken fiber is redistributed among the intact fibers. The subsequent load redistribution can lead to an entire avalanche of breakages, which can either stop after a certain number of consecutive failures, retaining the integrity of the bundle, or can be catastrophic, resulting in a macroscopic failure of the entire system. According to the strength of transverse association in the rupture process, the mechanism by which the extra stress caused by a fiber failure is redistributed among the intact fibers can be classified into several types. The most common one is global load sharing (GLS); that is, after each fiber failure, the released load is equally redistributed among all the intact fibers. The FBM in the GLS case assumes an interaction among the fibers with a mean field approximation and can often be solved analytically. On the other hand, the extreme case of a short-range interaction is local load sharing (LLS), which maintains stress concentration around the broken fibers. In this case, the extra load borne by the failing fibers is transferred to their nearest intact neighbors. Due to the nontrivial local spatial correlation, the exact solution of LLS bundles is nearly impossible [4]. In most cases, LLS models can only be treated through computer simulation. In some rare cases, their analytical solution is limited to the determination of asymptotic behaviors. In fact, some research shows that stress redistribution in actual heterogeneous materials should fall in many intermediate load sharing forms, such as power law redistribution rules [5].

In the failure process, the most important characteristic of the microscopic fracture mechanism is the size distribution of the burst avalanches, which can be monitored experimentally by acoustic emission techniques [6–8]. In the GLS limit, the avalanche size distributions of the classical FBM with various fracture threshold distributions follow a power law with a universal exponent $-5/2$ [9–11]. In the LLS case, however, the avalanche size distribution is more complicated, depending on the specific form of the threshold distribution [12,13]. The various macroscopic stretching and fracture natures of the actual materials can be described by the stress-strain relationship, by which different fracture properties of the materials can be intuitively divided into brittle, semibrittle, plastic, and so on. As the applied load increases quasistatically, there exists a critical stress σ_c, beyond which the catastrophic failure of the whole system takes place. Current studies on the FBM mainly involve describing the constitutive relationship, the determination of the critical stress σ_c, and the investigation of the phase transition from a state of partial failure to a state of complete failure.

In order to obtain a more realistic description for a wide range of composites, a series of deformation models based on the classical FBM have been introduced. Pradhan *et al.* [14–16] investigated the breakdown of a random fiber-bundle model with a lower cutoff in fiber threshold distribution both in the GLS and LLS cases. They found that the existence of a crossover behavior near fracture criticality makes it possible to predict the imminent global failure point of the system [17,18]. Raischel *et al.* [13] studied the failure properties of the fiber bundle with a finite lower cutoff of the strength disorder, varying the range of interaction between the limiting cases of GLS and LLS. Their computer simulations revealed that at interaction local load sharing, the avalanche distribution

*hdpcumt@126.com
†gangtang@cumt.edu.cn

of the FBM is much more complicated than that in GLS. Divakaran and Dutta [19,20] investigated the breakdown of a random fiber-bundle model with one or more discontinuities in the threshold distribution using the GLS scheme. These discontinuities significantly modify the avalanche size distribution. Some researchers have also considered the FBM with a continuous damage law; that is, the stiffness of the fibers gradually decreases in consecutive failure events before the final macroscopic rupture happens [21–25].

Recently, Halász and Kun [26,27] introduced the FBM with a stick-slip dynamics based on the classical FBM. In this model, the fiber is assumed to undergo several sliding events, which happen when the local load exceeds some threshold values and gradually increase the relaxed length of the fiber. Eventually a fiber might fail after a series of sliding events if the external load is large enough. In this model the Young modulus of a fiber is kept fixed throughout the whole process. On the macroscopic scale, by building the constitutive equation of the system, they showed analytically that the sliding mechanism leads to the macroscopic plasticity of the bundle and a permanent deformation which remains even after the load has been released. The model exhibits a broad spectrum of constitutive behaviors which can be controlled by varying certain parameters. These behaviors agree qualitatively with the measured response of stick-slip systems. On the microscopic scale, by varying the disorder property of the slip threshold and the maximum number of stick-slip events of a fiber, the system undergoes a transition from a phase where only small avalanches are formed to another one where a macroscopic slip appears.

However, some biological protein fibers, such as silk and spider silk fibers [28,29], show a hardening phenomenon along with the stick-slip dynamics. Some collagen materials [30,31] also show an increase of the Young modulus in the stretching process. In order to describe the change in the Young modulus along with the stick-slip dynamics in the stretching process, in this paper we consider an increase or decrease of the Young modulus of a fiber with stick-slip dynamics after local sliding events. So the maximum number of stick-slip events of a single fiber and the change ratio of the Young modulus are the two critical exponents of the model. By analysis and numerical simulation, we explore the constitutive law, the critical stress, the average size of the largest avalanche, the avalanche size distribution, and the step of external load increase influenced by the two main parameters of the model. Compared to the model with a constant Young modulus, the variable Young modulus in this model can describe prolific fracture properties of biological fibers [32,33].

II. THE AVALANCHE PROCESS OF THE FBM WITH STICK-SLIP DYNAMICS AND A VARIABLE YOUNG MODULUS

The FBM with stick-slip dynamics and a variable Young modulus is composed of fibers which can gradually increase their relaxed length when the local load exceeds some threshold values. Following a sliding event, the strength of a fiber accordingly changes, i.e., the Young modulus of a fiber increases or decreases by multiplying by a factor α. After a number of sliding events, the fiber will fail completely under a large enough external load, which is shown in Fig. 1. In detail, this model can be constructed as follows: The bundle consists of N parallel fibers, all with an identical Young modulus $E_f = 1$ at first, which are assembled on a one-dimensional lattice of length N. The bundle is supposed to be loaded parallel to fibers quasistatically. The fiber exhibits a linearly elastic behavior throughout the whole process except for a series of stick-slip events. When the deformation of a fiber reaches a series threshold values σ_i^j, a range of sliding events occur, where the index $i = 1,2,\ldots,N$, $j = 1,2,\ldots,K_{\max}$. The parameter $K_{\max}$ denotes the maximum number of slips allowed for a single fiber before its final failure, which is a key parameter of the model. After j times sliding events, the Young modulus changes to $\alpha^j E_f$. In the rear section of the failure process, this model can be seen as a fiber-bundle model with a random Young modulus [34]. In this model, we consider the annealed disorder, i.e., after each sliding event the fiber gets a new threshold value. The sliding threshold value σ_i^j of an individual fiber is an independent random variable with a probability density p and a cumulative probability distribution,

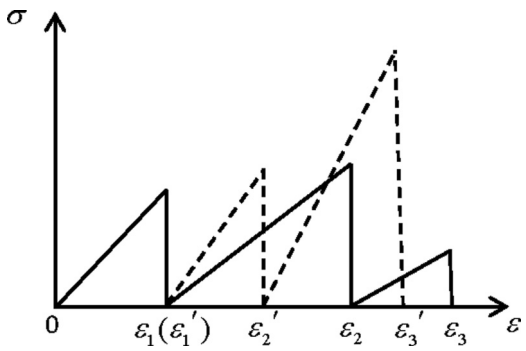

FIG. 1. The constitutive behavior of a fiber with stick-slip dynamics and a variable Young modulus. The dotted line indicates the case of the increasing Young modulus, and the solid line indicates the case of the decreasing Young modulus.

$$P(\sigma) = \int_0^\sigma p(x)dx. \tag{1}$$

In this paper, the threshold σ is assumed to have a Weibull distribution with a cumulative distribution function

$$P(\sigma) = 1 - \exp[-(\sigma/\lambda)^m]. \tag{2}$$

We assume $m = 2$, $\lambda = 1$ according to extensive research on the FBM. After $K_{\max}$ times sliding events, a final breaking occurs, and as a result, the strength of the fiber becomes zero. At a certain macroscopic deformation ε, the load undertaken by a fiber after j times sliding events can be described as

$$f_j = \alpha^j E_f(\varepsilon - \varepsilon_1 - \varepsilon_2 - \cdots - \varepsilon_j), \tag{3}$$

where ε_j represents the corresponding strain threshold of the jth sliding event of the fiber. After a sliding or fracture event, the released load is equally redistributed among all the unbroken fibers. In the simulation, the load is increased quasistatically, i.e., the load is increased to bring only the weakest unbroken fiber to slide or break. In order to get reliable results, we identify the number of fibers $N = 100\,000$; the following results are an average of at least 2000 simulations.

In general, the classical FBM in the limiting case of GLS can be solved analytically. For the classical FBM in the GLS case, the stress-strain relationship can be expressed as

$$f = F/N = \varepsilon[1 - P(\varepsilon)], \tag{4}$$

which can describe the FBM without the stick-slip dynamics. If fibers are allowed to slide only once before their final failure, the fibers can be classified as two parts: The parts of the fibers with sliding thresholds $\sigma \geqslant E\varepsilon$ are still intact and can bear the local load $E\varepsilon$, while those fibers with $\sigma < E\varepsilon$ have already undergone a sliding event, keeping local load $\alpha E(\varepsilon - \varepsilon_1)$. So the macroscopic stress-strain relationship can be spread as

$$F/N = \varepsilon[1 - P(\varepsilon)] + \int_0^{\varepsilon} p(\varepsilon_1) d\varepsilon_1 \alpha(\varepsilon - \varepsilon_1) \times [1 - P(\alpha(\varepsilon - \varepsilon_1))]. \tag{5}$$

In more general cases, if the fiber can slide $K_{\max}$ times before its final failure, the constitutive relationship can be expressed as

$$\frac{F}{N} = f(\varepsilon) = f_0(\varepsilon) + f_1(\varepsilon) + f_2(\varepsilon) + \cdots + f_{K_{\max}}(\varepsilon), \tag{6}$$

where $f_K(\varepsilon)$ represents the load borne by fibers that have just slide K times. In detail, $f_0(\varepsilon) = \varepsilon[1 - P(\varepsilon)]$,

$$f_K(\varepsilon) = \int_0^{\varepsilon} \int_0^{\varepsilon-\varepsilon_1} \cdots \int_0^{\varepsilon-\varepsilon_1\cdots-\varepsilon_{K-1}} \prod_{i=1}^{K} d\varepsilon_i \, p(\alpha^{i-1}\varepsilon_i) \times \alpha^K \left(\varepsilon - \sum_{j=1}^{K} \varepsilon_j\right) \left[1 - P\left(\alpha^K \left(\varepsilon - \sum_{j=1}^{K} \varepsilon_j\right)\right)\right]. \tag{7}$$

The macroscopic constitutive relationship in the tensile fracture process can be obtained by a numerical solution of Eq. (6).

On the microscopic level, the approximate analysis results of avalanche size distribution can be deduced according to Ref. [21]. For the classical FBM in the GLS case, Hemmer and Hansen [9,12] have proved that the probability density $D(\Delta)$ for the avalanche size Δ during a quasistatic loading process can be calculated by using the integral form

$$D(\Delta) = \frac{\Delta^{\Delta-1}}{\Delta!} \int_0^{\varepsilon_m} p\left(\frac{\varepsilon}{\sum_{i=1}^{K+1} \frac{1}{\alpha^{i-1}}}\right) (1 - a_\varepsilon) a_\varepsilon^{\Delta-1} e^{-\Delta a_\varepsilon} d\varepsilon, \tag{8}$$

where ε denotes the macroscopic deformation of the bundle. ε_m denotes the maximum value of the deformation which corresponds to the final failure of the whole bundle. a_ε is the average fraction of broken fibers following an infinitesimal increase in the deformation ε of the bundle.

The probability density that a fiber will slide again after sliding k times under an infinitesimal strain increase can be expressed as

$$p_k^{k+1}(\varepsilon) = \frac{d}{d\varepsilon} \int_0^{\varepsilon} \int_0^{\varepsilon-\varepsilon_1} \cdots \int_0^{\varepsilon-\varepsilon_1\cdots-\varepsilon_{K-1}} \prod_{i=1}^{K} d\varepsilon_i \, p(\alpha^{i-1}\varepsilon_i). \tag{9}$$

Following this failure event, the fiber can release stress $\delta f = \alpha^K(\varepsilon - \sum_{j=1}^{K} \varepsilon_j)$, which will be distributed among the residual fibers. As a result of the distribution of released stress, the deformation increase of the unfaulted fibers can be expressed as

$$\delta\varepsilon = \frac{\delta f}{Y(\varepsilon)} = \frac{\alpha^K}{Y(\varepsilon)} \left(\varepsilon - \sum_{j=1}^{K} \varepsilon_j\right), \tag{10}$$

where $Y(\varepsilon)$ represents the effective Young modulus of the bundle at the deformation ε, which can be obtained by the relationship $f = Y(\varepsilon)\varepsilon$. So at the strain ε, the total probability that a fiber breaks as a consequence of another fiber breaking reads as

$$p_{\text{tot}}(\varepsilon) = p_k^{k+1}(\varepsilon)\delta\varepsilon = \frac{d}{d\varepsilon} \int_0^{\varepsilon} \int_0^{\varepsilon-\varepsilon_1} \cdots \int_0^{\varepsilon-\varepsilon_1\cdots-\varepsilon_{K-1}} \times \prod_{i=1}^{K} d\varepsilon_i \, p(\alpha^{i-1}\varepsilon_i) \left(\varepsilon - \sum_{j=1}^{K} \varepsilon_j\right) \frac{\alpha^K}{Y(\varepsilon)}, \tag{11}$$

which is another expression of a_ε in Eq. (8). So the avalanche size distribution can be obtained by computing the probability $D(\Delta)$ for various sizes of avalanche Δ.

A. The impacts of $K_{\max}$

The macroscopic constitutive behaviors of the FBM with stick-slip dynamics and a variable Young modulus at different $K_{\max}$ values are obtained both analytically and numerically. The constitutive behaviors are provided and compared in Figs. 2 and 3 for $\alpha = 0.8$ and $\alpha = 1.2$, respectively. From the four figures, one can observe that the change in Young modulus and the maximum sliding number $K_{\max}$ can have a significant influence on the constitutive relationship. In the small region of $K_{\max}$, the constitutive curves have a similar shape both at $\alpha = 0.8$ and $\alpha = 1.2$. While $K_{\max}$ increases, the influence of the Young modulus transformation becomes more apparent. As shown in Fig. 2, when the Young modulus decreases in the sliding process, both the analysis and the simulation results show that the maximum deformation corresponding to the whole failure can observably increase following the increase of $K_{\max}$. In Fig. 2(b), when $K_{\max}$ is small, the constitutive curve has a relatively sharp maximum. As $K_{\max}$ increases, there appears a progressively more obvious plastic plateau whose length increases with increasing $K_{\max}$, while for the analysis results in Fig. 2(a), there is no obvious plastic plateau in the constitutive curves. The difference between the analysis results and the simulation results mainly arise from the combined effect of the approximation in the analytical method and the deviation in numerical integration. In the case of a Young modulus increasing in the sliding process, which is shown in Fig. 3, constitutive curves are unimodal. At the initial strain stage before the whole failure, the maximum stress increases with increasing $K_{\max}$, while in the large region of strain, the constitutive laws all have the same asymptotic behaviors for various $K_{\max}$ in both analysis and simulation results.

In the failure process, the critical stress σ_c is defined as the maximum load that the system can support before its final breakdown. The critical stress as a function of $K_{\max}$ is presented in Fig. 4. When $\alpha = 0.8$, for small $K_{\max}$, the critical

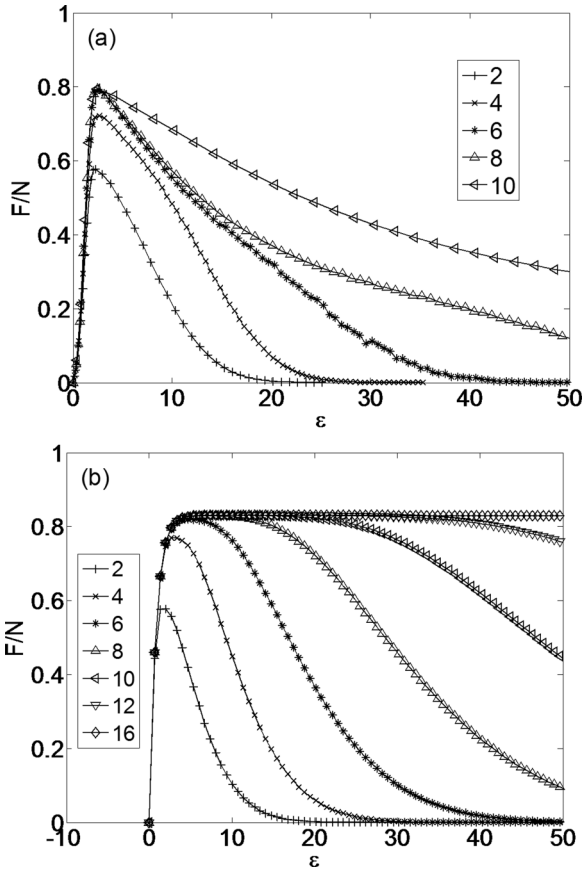

FIG. 2. The constitutive behavior of the model with $\alpha = 0.8$ for several different values of $K_{\max}$. (a) Analysis results; (b) simulation results.

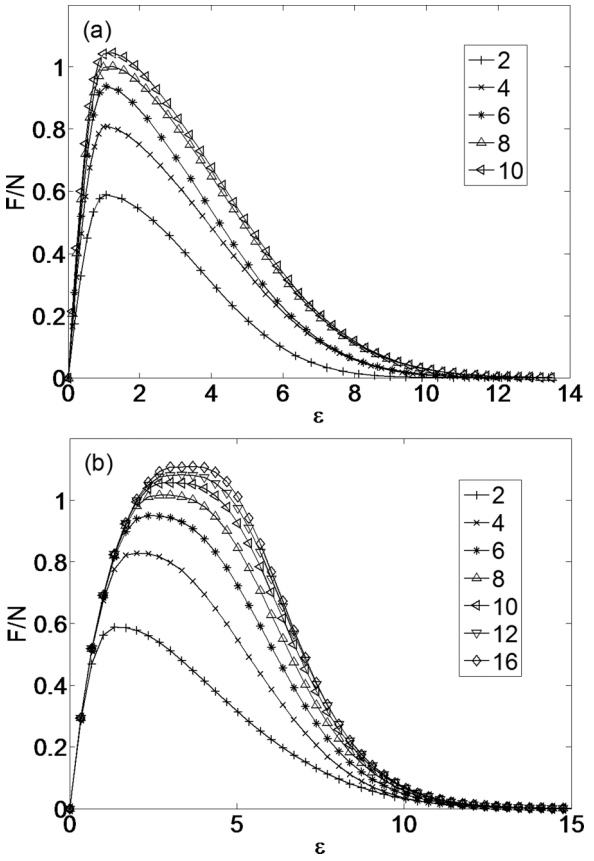

FIG. 3. The constitutive behavior of the model with $\alpha = 1.2$ for several different values of $K_{\max}$. (a) Analysis results; (b) simulation results.

stress increases monotonously with increasing $K_{\max}$. However, as $K_{\max}$ increases, the critical stress reaches a saturation value. When $\alpha = 1.2$, which means the Young modulus increases in the sliding process, the critical stress increases monotonously with increasing $K_{\max}$ in the limit of the simulation. We can imagine that the critical stress at $\alpha = 1.2$ will also reach a saturation value if the $K_{\max}$ continues to increase. Comparatively speaking, in the case of $\alpha = 1.2$, the diversity between analysis results and simulation results is much smaller than the one in the case of $\alpha = 0.8$, which is in accordance with the constitutive curves on Figs. 2 and 3. In short, the change of the Young modulus has a large impact on the macroscopic tensile properties of the model. In the case of decreasing Young modulus, the maximum sliding number $K_{\max}$ mainly affects the maximum strain in the sliding process, however, in the case of increasing Young modulus, $K_{\max}$ mainly affects the critical stress.

In Fig. 5, the normalized average size of the largest avalanche $\langle \Delta_m \rangle / N$ is plotted as a function of $K_{\max}$. When $K_{\max}$ is small, the value of $\langle \Delta_m \rangle$ increases rapidly with increasing $K_{\max}$. As $K_{\max}$ approaches 8, $\langle \Delta_m \rangle$ increases more slowly and will reach a saturation value as $\alpha = 0.8$. When $\alpha = 1.2$, there is only a trend of saturation in the large limit of $K_{\max}$ within our simulation. The obvious reason for the trend of saturation is that the avalanche size cannot increase continuously as increasing $K_{\max}$ for the limitation of the bundle size N. So the avalanche size has a saturation value when its value is close to the size of the bundle. The relationship of $\langle \Delta_m \rangle$ and $K_{\max}$ shows that as $K_{\max}$ increases, the avalanche process becomes progressively more concentrative.

The avalanche size distributions of the model at $\alpha = 0.8$ and $\alpha = 1.2$ are analytically and numerically studied, and the results are exhibited in Figs. 6 and 7, respectively. It is important to emphasize that the curves in all cases can be well fitted with a power law asymptotic behavior, similarly to the other classical FBM in the GLS case:

$$D(\Delta) \sim \Delta^{-\xi}. \tag{12}$$

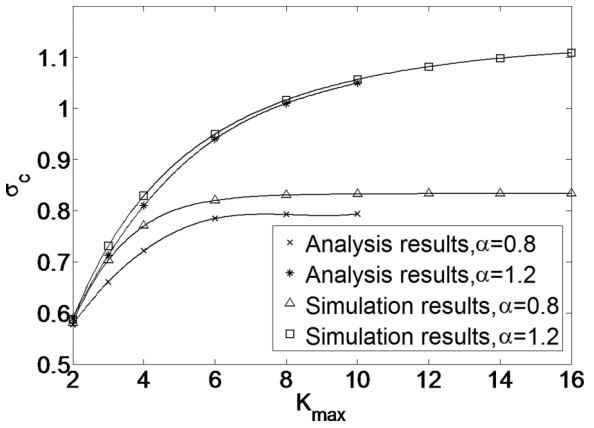

FIG. 4. The critical stress of the model as a function of $K_{\max}$.

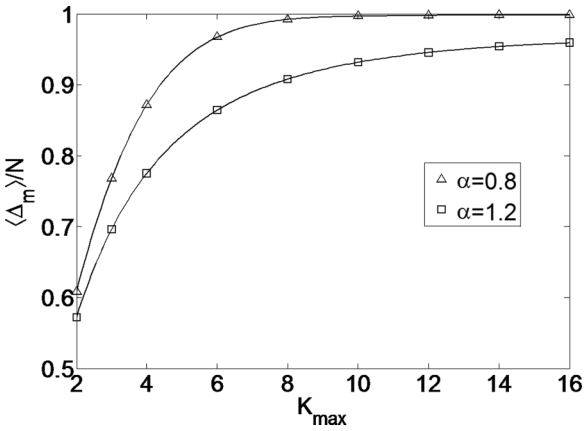

FIG. 5. The normalized average size of the largest avalanche of the model as a function of $K_{\max}$.

The presence of the stick-slip dynamics does not hinder the power law of the avalanche size distribution in the FBM with GLS. In Fig. 6(a), the analysis results show that the upper curve corresponding to $K_{\max} = 2$ can be fitted by the power law with an exponent $\xi = 2.5$, while when $K_{\max} = 10$, the exponent $\xi = 1.9$. In Fig. 6(b), for the simulation results, the

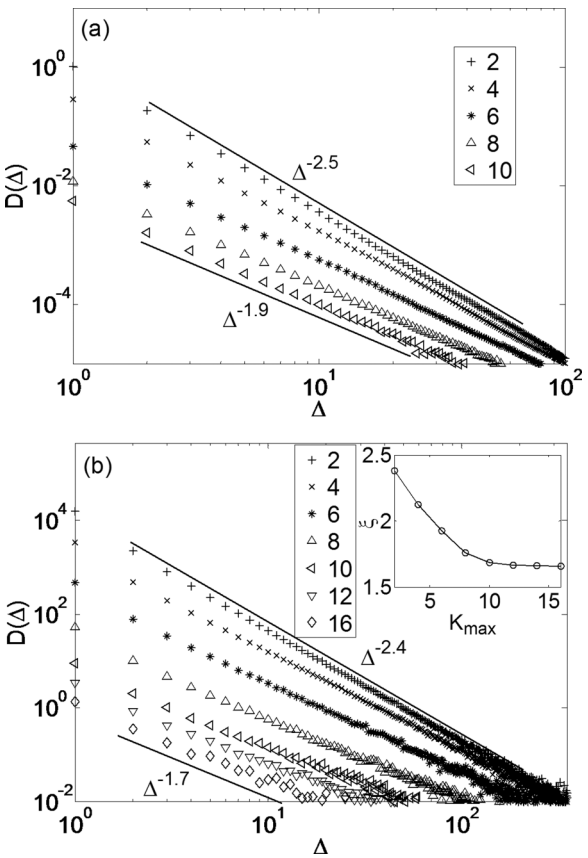

FIG. 6. Avalanche size distribution of the model with $\alpha = 0.8$. (a) Analysis results; the straight lines denoting the power law with slope -1.9 and -2.5 are also shown. (b) Simulation results; the straight lines denoting the power law with slope -1.7 and -2.4 are also shown. In the inset of (b), the exponents of the power law as a function of $K_{\max}$ are presented.

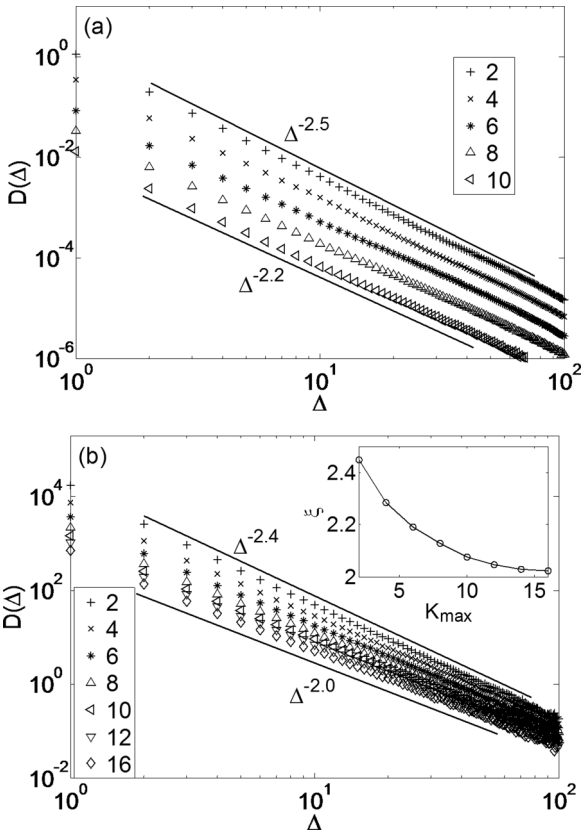

FIG. 7. Avalanche size distribution of the model with $\alpha = 1.2$. (a) Analysis results; the straight lines denoting the power law with slope -2.2 and -2.5 are also shown. (b) Simulation results; the straight lines denoting the power law with slope -2.0 and -2.4 are also shown. In the inset of (b), the exponents of the power law as a function of $K_{\max}$ are presented.

exponents corresponding to $K_{\max} = 2$ and 16 are $\xi = 2.4$ and $\xi = 1.7$. Correspondingly, in Fig. 7, the exponents from analysis results are $\xi = 2.5$ and $\xi = 2.2$ corresponding to $K_{\max} = 2$ and $K_{\max} = 10$, while for simulation results, the exponents corresponding to $K_{\max} = 2$ and $K_{\max} = 16$ are $\xi = 2.4$ and $\xi = 2.0$. Figures 6 and 7 show that for the microscopic statistical properties of the breaking process, the analysis results are consistent with the simulation results in a quantitative manner. When $K_{\max}$ increases from 2, there is a crossover in the distribution of avalanche size. This crossover behavior indicates that the avalanche process is obviously affected by the value of $K_{\max}$. As $K_{\max} = 2$, in spite of the Young modulus increasing or decreasing, the avalanche size distribution is close to the one in the classical FBM. The only minor difference in exponents of the power law is due to the two times sliding events. The insets of Figs. 6(b) and 7(b) show exponents of the power law as a function of $K_{\max}$ by the simulation method. In the small region of $K_{\max}$, the exponents decrease rapidly with increasing $K_{\max}$, however, in the large limit of $K_{\max}$, the exponents approach a limited value depending on the change in the Young modulus. In comparison, in the case of the decreasing Young modulus, the value of $K_{\max}$ can have more significant impacts on the avalanche size distribution than that in the case of increasing

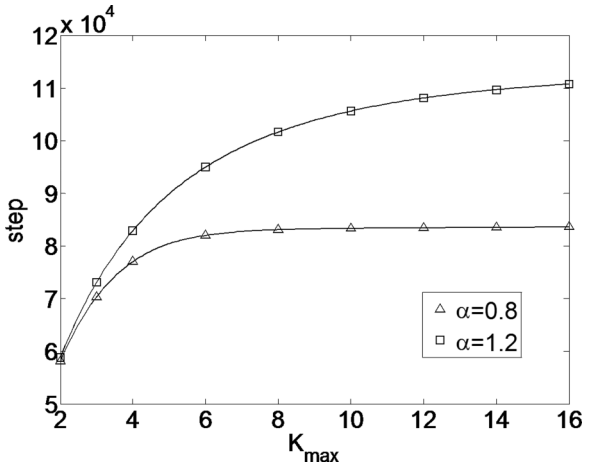

FIG. 8. The total steps of load increase until final failure as a function of $K_{\max}$.

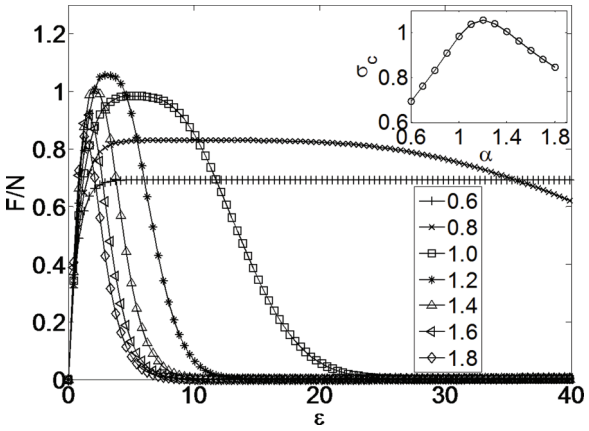

FIG. 9. The constitutive behavior of the model with $K_{\max} = 10$ for several different values of α. In the inset the critical stress as a function of α is presented.

Young modulus. From the above analysis, we find that there is no universal behavior of the avalanche size distribution in the FBM with stick-slip dynamics and a variable Young modulus.

In the failure process, the step number of the external load increases before the final catastrophic failure can reflect the relaxation process of the material fracture. At each step of such a load increment only one fiber fails. It can be assumed that the external loads have to increase x times before the final complete failure. The relationship between the step of load increase and the value of $K_{\max}$ by the simulation method is illustrated in Fig. 8. When $K_{\max} > 6$, the step number reaches a saturation value of $\alpha = 0.8$, while for $\alpha = 1.2$ there is only a trend of saturation in the large limit of the $K_{\max}$ value. When $\alpha = 0.8$, the number of stick-slip events can only exert a very limited influence on the step of load increase. Although the microcosmic avalanche size distribution has a significant crossover behavior, the macroscopic tensile fracture properties such as the critical stress and the step of load increase will quickly reach a saturation value as $K_{\max}$ keeps increasing.

B. The impacts of α

As we can see in the above discussion, the maximum number of stick-slip events of a single fiber can have dramatic impacts on the failure process of the model. At the same time, the variation of the Young modulus can also have a remarkable influence on the properties of the model. In the following investigation, the impacts of the ratio α on the macroscopic and microscopic properties of the model are studied through a simulation method with a defined $K_{\max}$. In order to ensure sufficient effects of the stick-slip dynamics, the maximum sliding number $K_{\max}$ is assumed to be 10.

The macroscopic constitutive behaviors of the model with $K_{\max} = 10$ for different values of α are provided in Fig. 9. When $\alpha < 1$, the constitutive relations show an apparent local plateau regime which indicates a plastic response of the bundle. At the same time, the maximum deformation corresponding to the final macroscopic fracture increases rapidly with decreasing α. When $\alpha > 1$, the local plastic state disappears gradually. With increasing α, the maximum peaks in the constitutive curves become progressively more pointed. The above descriptions demonstrate that a decline of the Young modulus leads to a local plastic state, however, an increase of the Young modulus corresponds to the brittle condition in the failure process with stick-slip dynamics. From Fig. 9 we can see that α can exert a complicated impact on the maximum load. The critical stress as a function of the changing ratio of the Young modulus α is shown in the illustration. When $\alpha < 1.2$, the critical stress increases approximately linearly with α until it reaches a maximum peak at $\alpha = 1.2$. When α becomes larger than 1.2, the critical stress declines again. The results indicate that an overlarge or too small changing amplitude of the Young modulus will block the strength enhancement of the FBM with stick-slip dynamics.

The influence of α on the microscopic properties of the failure process is displayed by the avalanche size distribution in Fig. 10. We can find intuitively that the distributions can be well fitted with a power law asymptotic behavior similar to the classical FBM in GLS. The major impact of the ratio α is mainly reflected in the exponents of the power law distribution.

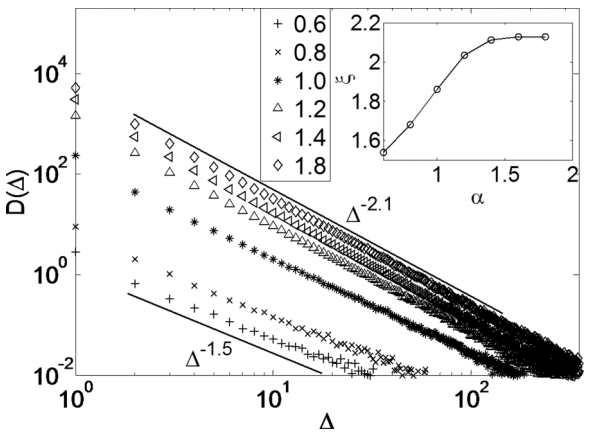

FIG. 10. Avalanche size distribution of the model with $K_{\max} = 10$. The straight lines denoting the power law with slope -1.5 and -2.1 are also shown. In the inset, the exponents of the power law as a function of α are presented.

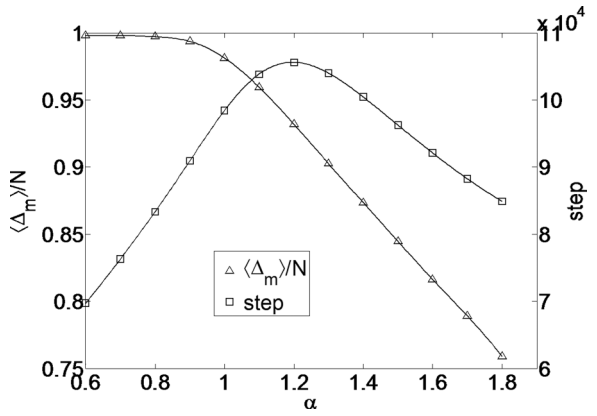

FIG. 11. The normalized average size of the largest avalanche (Δ) and the total steps of load increase until final failure ($\square$) as a function of α in the model with $K_{\max} = 10$.

The lower curve corresponding to $\alpha = 0.6$ can be fitted by the power law with an exponent $\xi = 1.5$, while in the large α limit, the exponent $\xi = 2.1$. The inset of Fig. 10 shows the exponents of the power law as a function of α. In the small region of α, the exponents increase rapidly with increasing α, however, for the larger α, the exponents approach a saturation value. When α is close to 1, the value of α has a significant impact on the avalanche size distribution, which reflects the influence of α on the microcosmic fracture mechanism of loaded fibers. The impacts of $K_{\max}$ and α on the avalanche size distribution indicate that when the Young modulus is constant, the results in this paper are well consistent with the size distribution of slip avalanches in the FBM with stick-slip dynamics [27].

The normalized average size of the largest avalanche as a function of α is displayed in Fig. 11, and, in the same figure, the total steps of load increase until final failure is also showed. When $\alpha < 1$, which means the Young modulus declines in the sliding process, the average size of the largest avalanche $\langle \Delta_m \rangle$ is almost independent of α, while in the larger region of α, $\langle \Delta_m \rangle$ declines almost linearly with increasing α. The relationship of $\langle \Delta_m \rangle$ and α shows that the spatial association strength of the system will decrease with increasing Young modulus. The total steps of the load increase can reflect the relaxation process of the fracture. As we can see from the Fig. 11, there is a maximum peak in the step curve at $\alpha = 1.2$, which means that the FBM with stick-slip dynamics has the highest stability in this condition.

III. DISCUSSION AND CONCLUSIONS

In this paper, we construct an improved FBM with stick-slip dynamics to describe a wider range of biological fibers. Unlike in the original FBM with stick-slip dynamics, the Young modulus of a fiber is not fixed, but rather variable, either increasing or decreasing after a local sliding event. The maximum number of stick-slip events of a single fiber $K_{\max}$ and the change ratio of Young modulus α are the two key parameters of the model. For stress controlled experiments, both the macroscopic constitutive behavior and the microscopic damage process are studied for various α and $K_{\max}$, both analytically and numerically.

Both the analytical and the numerical results show that the value of $K_{\max}$ has a significant effect on the model both macroscopically and microscopically. We studied this effect for two different cases. In one case the Young modulus of a fiber decreases after each sliding event, while in the other it decreases. In the case of decreasing Young modulus, varying the value of $K_{\max}$ mainly alters the critical fracture strain in constitutive curves. The critical stress, the average size of the largest avalanche, and the step number of load increase all saturate when $K_{\max}$ increases to 10, while in the case of increasing Young modulus, $K_{\max}$ mainly affects the critical stress in a macroscopic manner. Furthermore, unlike in the previous case, the critical stress, the average size of the largest avalanche, and the step number of load increases never really saturate in the large limit of $K_{\max}$ within our simulation, although they do show a trend of saturation. In the aspect of microfracture mechanism, the appearance of stick-slip dynamics does not hinder the power law distribution of the avalanche size in the FBM model with GLS. Both at $\alpha = 0.8$ and $\alpha = 1.2$, the exponents of the power law are all monotonic decreasing functions of $K_{\max}$, while both the critical stress and the step number of load increases are monotonic increasing functions of $K_{\max}$, which implies that the intensity and the stability of the system are enhanced if $K_{\max}$ increases. The analytical and the simulation results agree with each other quantitatively, although there exist tiny discrepancies between the two, which we suspect come from the combined effect of the approximation in the analytical method and the deviation in the numerical integration.

The impacts of α on the model are illustrated in Figs. 9–11. The constitutive curve shows that for $\alpha < 1.0$ the material exhibits excellent plasticity locally, and for $\alpha > 1.0$ its brittle characteristic becomes apparent. Therefore, if the Young modulus declines in the sliding process, the maximum deformation of the material at the final failure is very remarkable. Microscopically, the avalanche size distributions can be always well fitted into a power law no matter the value of the Young modulus, although the change ratio α does affect the power law exponents. As α increases, the average size of the largest avalanche decreases, signaling a decrease of the spatial association strength of the system. The maximum peak in the relationship between the total steps of load increase and α shows that the model has the highest stability at $\alpha = 1.2$.

In summary, we successfully constructed a FBM model with stick-slip dynamics and a viable Young modulus. Using this improved model we are able to describe more accurately the intricate behavior of various biological fibers. This theoretical study should be helpful for understanding the fracture process of a large range of biological materials.

ACKNOWLEDGMENTS

We sincerely thank Dr. L. M. Chen for his valuable discussions and kind help. This work was supported by the Fundamental Research Funds for the Central Universities (Grant No. 2012QNA51) and the National Science Foundation of China (Grants No. 11247029 and No. 11247249)

[1] B. K. Chakrabarti and L. G. Benguigui, *Statistical Physics of Fracture and Breakdown in Disorder Systems* (Oxford University Press, Oxford, UK, 1997).
[2] P. C. Hemmer, A. Hansen, and S. Pradhan, Lect. Notes Phys. **705**, 27 (2007).
[3] M. J. Alava, P. K. Nukala, and S. Zapperi, Adv. Phys. **55**, 349 (2006).
[4] S. Pradhan, A. Hansen, and B. K. Chakrabarti, Rev. Mod. Phys. **82**, 499 (2010).
[5] G. G. Batrouni, A. Hansen, and J. Schmittbuhl, Phys. Rev. E **65**, 036126 (2002).
[6] A. Garcimartin, A. Guarino, L. Bellon, and S. Ciliberto, Phys. Rev. Lett. **79**, 3202 (1997).
[7] A. Guarino, A. Garcimartin, and S. Ciliberto, Eur. Phys. J. B **6**, 13 (1998).
[8] C. Maes, A. Van Moffaert, H. Frederix, and H. Strauven, Phys. Rev. B **57**, 4987 (1998).
[9] P. C. Hemmer and A. Hansen, J. Appl. Mech. **59**, 909 (1992).
[10] S. Zapperi, P. Ray, H. E. Stanley, and A. Vespignani, Phys. Rev. Lett. **78**, 1408 (1997).
[11] S. Zapperi, P. Ray, H. E. Stanley, and A. Vespignani, Phys. Rev. E **59**, 5049 (1999).
[12] M. Kloster, A. Hansen, and P. C. Hemmer, Phys. Rev. E **56**, 2615 (1997).
[13] F. Raischel, F. Kun, and H. J. Herrmann, Phys. Rev. E **74**, 035104 (2006).
[14] S. Pradhan, P. Bhattacharyya, and B. K. Chakrabarti, Phys. Rev. E **66**, 016116 (2002).
[15] S. Pradhan and P. C. Hemmer, Phys. Rev. E **79**, 041148 (2009).
[16] S. Pradhan and A. Hansen, Phys. Rev. E **72**, 026111 (2005).
[17] S. Pradhan, A. Hansen, and P. C. Hemmer, Phys. Rev. Lett. **95**, 125501 (2005).
[18] S. Pradhan and B. K. Chakrabarti, Lect. Notes Phys. **705**, 459 (2007).
[19] U. Divakaran and A. Dutta, Phys. Rev. E **75**, 011117 (2007).
[20] U. Divakaran and A. Dutta, Phys. Rev. E **78**, 021118 (2008).
[21] R. C. Hidalgo, F. Kun, K. Kovács, and I. Pagonabarraga, Phys. Rev. E **80**, 051108 (2009).
[22] R. C. Hidalgo, F. Kun, and H. J. Herrmann, Phys. Rev. E **64**, 066122 (2001).
[23] F. Kun, S. Zapperi, and H. J. Herrmann, Eur. Phys. J. B **17**, 269 (2000).
[24] F. Raischel, F. Kun, and H. J. Herrmann, Phys. Rev. E **77**, 046102 (2008).
[25] D. P. Hao, G. Tang, H. Xia, K. Han, and Z. P. Xun, J. Stat. Phys. **146**, 1203 (2012).
[26] Z. Halász and F. Kun, Phys. Rev. E **80**, 027102 (2009).
[27] Z. Halász and F. Kun, Europhys. Lett. **89**, 26008 (2010).
[28] T. Seydel, W. Knoll, I. Greving, C. Dicko, M. M. Koza, I. Krasnov, and M. Müller, Phys. Rev. E **83**, 016104 (2011).
[29] M. Elices, G. V. Guinea, J. Pérez-Rigueiro, and G. R. Plaza, Mater. Sci. Eng., C **31**, 1184 (2011).
[30] B. A. Roeder, K. Kokini, J. E. Sturgis, J. P. Robinson, and S. L. Voytik-Harbin, J. Biomech. Eng. **124**, 214 (2002).
[31] M. E. Susilo, B. A. Roeder, S. L. Voytik-Harbin, K. Kokini, and E. A. Nauman, Acta Biomater. **6**, 1471 (2010).
[32] F. Bosia, M. J. Buehler, and N. M. Pugno, Phys. Rev. E **82**, 056103 (2010).
[33] F. Chen, D. Porter, and F. Vollrath, Phys. Rev. E **82**, 041911 (2010).
[34] E. Karpas and F. Kun, Europhys. Lett. **95**, 16004 (2011).